Microhardness of gas-dynamic coatings from aluminum powder multi-reinforced with fullerenes and aluminum oxide

A. V. Aborkin, *Candidate of Technical Sciences, Associated Professor, Department of Technology of Mechanical Engineering*[1], *e-mail: aborkin@vlsu.ru*
D. M. Babin, *Senior Researcher*[1], *e-mail: necros-m2@yandex.ru*
A. I. Elkin, *Candidate of Technical Sciences, Associated Professor, Head of Department of Technology of Mechanical Engineering*[1], *e-mail: elkin@vlsu.ru*
V. V. Ryabkova, *Junior Researcher*[1], *e-mail: vvryabkova@mail.ru*

[1] *Vladimir State University named after Alexander and Nikolay Stoletovs, Vladimir, Russia.*

This study presents data on the influence of aluminum oxide content in the powder mixture on the microhardness of gas-dynamic coatings based on the nanocomposite powder AlMg6/C_{60}. The synthesis of the powders was carried out through a two-stage high-energy processing of the initial components in a planetary ball mill. Powder characterization was conducted using scanning electron microscopy, granulometric analysis, and *X*-ray phase analysis. The obtained powders were used for cold gas-dynamic spraying. Microstructure analysis of the coatings revealed a uniform distribution of reinforcing particles throughout their volume. It was established that the addition of 10–50 wt.% Al_2O_3 into the powder mixture, along with mechanical treatment in the planetary mill, increases the coating's microhardness by approximately 30–45% compared to the material reinforced solely with C_{60}.

Key words: gas-dynamic spraying, coatings, fullerenes, microhardness, structure.
DOI: 10.17580/nfm.2024.02.08

Introduction

One of the promising methods for creating coatings on the working surfaces of machine parts is cold gas-dynamic spraying [1–4]. The main advantage and distinguishing feature of cold gas-dynamic spraying, compared to other coating methods, is that during the process, high-velocity deformation of powder particles occurs while they remain in the solid phase [5]. This makes it highly effective for producing coatings, including those based on nanocrystalline powders.

A major drawback of aluminum-based powder coatings and their alloys, which limits their broader application, is their low microhardness, typically not exceeding ~100–150 HV [6, 7]. Overcoming this limitation is possible through the development of composite coatings, such as by reinforcing the aluminum matrix with ceramic particles [8, 9]. However, the potential for improving coating properties through the introduction of ceramic microparticles is currently limited, if not exhausted.

As a result, new prospects for enhancing and tailoring the desired set of properties arise from the development of multi-reinforced coatings with two or more types of reinforcing additives. In this regard, it is particularly viable to create coatings with a nanocrystalline matrix material structure containing both nano- and microscale reinforcement [10]. The production of multi-reinforced powders can be achieved by introducing reinforcing particles into the matrix material through high-energy ball milling. By controlling the conditions of high-energy milling, as well as the type and fraction of reinforcing particles, it is possible to purposefully design structures at both the nano- and microscale levels.

Among the promising nanoscale fillers that contribute to the enhancement of the physical and mechanical properties are fullerenes [11–14]. As for ceramic particles, aluminum oxide has proven to be highly effective in creating tribological coatings [15–17].

The present study focuses on the synthesis and characterization of powders based on the aluminum alloy AlMg6, multi-reinforced with fullerenes and aluminum oxide, as well as the investigation of the structure and microhardness of the coatings produced from these powders.

Methods of acquisition and characterization

The process of obtaining multi-reinforced powders consisted of two stages. In the first stage, a composite nanostructured powder based on the AlMg6 aluminum alloy, reinforced with fullerene C_{60}, was produced. The AlMg6/C_{60} nanocomposite powder was obtained through the joint mechanical processing of the initial components in a high-energy planetary ball mill AGO-2U. A mixture of AlMg6 alloy chips with the addition of 0.3 wt.% fullerene C_{60} was processed at a carrier rotation speed of 1800 rpm for 60 minutes in a steel grinding container using 8 mm diameter steel balls. The ratio of the mass of the processed charge to the mass of the balls was 1 : 20. To maintain the required thermal regime of the process, high-energy ball milling was performed in cycles of 5 minutes with 3-minute pauses. As a result,

the obtained powder mixture consisted of particles (agglomerates) no larger than 300 μm in size, composed of the AlMg6 matrix alloy and fullerenes. The particles (agglomerates) had a rounded shape with a developed surface. A detailed characterization of the AlMg6/C_{60} composite powder obtained in the first processing stage is provided in [18].

In the second stage, 10, 30, and 50 wt.% of Al_2O_3 particles with an average size of 18.5 μm were added to the obtained AlMg6/C_{60} nanocomposite powder (see **Fig. 1**). The mixtures were placed in a ceramic grinding container and processed in a FRITSCH PULVERISETTE 6 planetary ball mill at a carrier rotation speed of 600 rpm for 15 minutes using 8 mm diameter ceramic balls. Coatings from the obtained multi-reinforced powders were formed using the low-pressure cold gas dynamic spraying method. For this purpose, the DIMET-404 system was used. The selection of spraying parameters was guided by the data from works [19]. The spraying was performed on St08kp steel substrates. Air at a pressure of 0.8 MPa was used as the working gas. The air flow temperature was 450 °C. The spraying was performed in a fixed point, i. e., without nozzle movement (stationary mode). The powder feed exposure time was 15 seconds. The distance from the nozzle outlet to the substrate surface was 10 mm.

The morphology of the synthesized powders was studied using a LEO 1450 VP scanning electron microscope

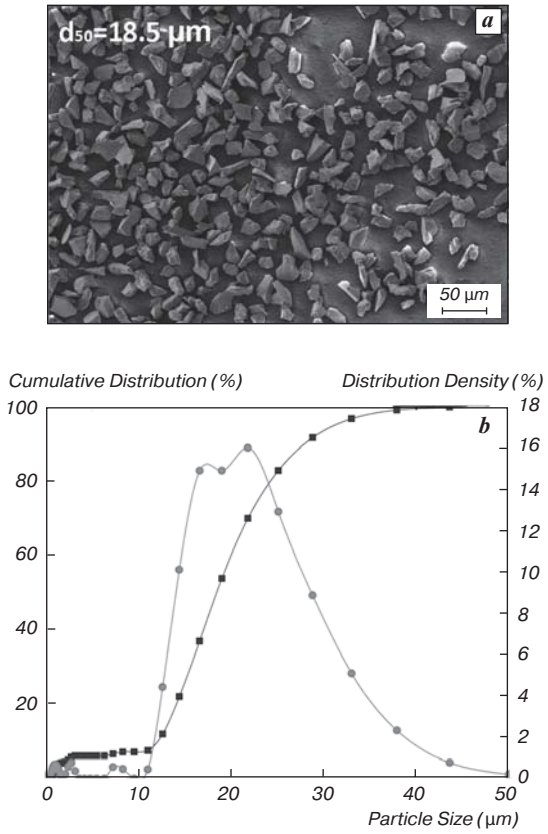

Fig. 1. SEM images (*a*) and particle size analysis data (*b*) of the initial powder Al_2O_3

equipped with an INCA 300 energy dispersive *X*-ray spectroscopy (EDS) detector. The particle size distribution of the obtained multi-reinforced powders was determined using a Microsizer-201C. The structural and phase composition of the powders was investigated by *X*-ray diffraction analysis on a D8 ADVANCE system. The quantitative determination of Al_2O_3 content in the coating was performed by processing the *X*-ray diffraction data using the reference intensity ratio method with DIFFRAC.EVA v2.0 software and ICDD PDF2 database. The size of coherent scattering regions was calculated using the Scherrer equation. The volume-averaged sizes of the coherent scattering regions were calculated based on the assumption of a spherical crystallite shape. The microhardness of the powder particles and coatings was measured by the kinetic indentation method using a Micro-Combi Tester (CSM Instruments) on cross-sectional samples. The measurements were carried out using a Vickers indenter with a load of 0.1 N and a dwell time of 10 s. No fewer than 10 measurements were performed.

Results and discussion

Fig. 2 presents the SEM images of multi-reinforced powder mixtures with 10, 30, or 50 wt.% Al_2O_3, obtained after the second stage of high-energy ball milling. The analysis of the SEM images of the multi-reinforced powders with varying ceramic particle content reveals significant differences. For instance, in the mixture containing 10 wt.% Al_2O_3, a low number of free ceramic particles can be observed. In this case, the ceramic particles are almost entirely distributed on the surface of the AlMg6 matrix alloy or embedded within it (see **Fig. 2, *a***). The small quantity of free ceramic particles in the powder mixture is likely to lead to reduced coating growth efficiency during cold spraying at low pressure conditions [20]. In contrast, for compositions containing 30 or 50 wt.% Al_2O_3 (see **Fig. 2, *b*, *c***), a different pattern emerges. A significant increase in the number of free ceramic particles is observed, which grows as their content in the powder mixture increases. This suggests the presence of a "saturation threshold" at which the surface of the matrix alloy particles is almost entirely covered by hard ceramic inclusions. This either halts or, at the very least, hinders the embedding of ceramic particles into the ductile matrix alloy. Additionally, the surface of the matrix alloy particles becomes more developed due to the deformation effects of the ceramic particles during ball milling. Submicron and micron-sized matrix material particles form through micro-cutting by the harder ceramic particles on the surface of the matrix alloy particles. This process also leads to an increase in the specific surface area of the powder, potentially promoting the growth of the volumetric fraction of native aluminum oxide, as evidenced by the increase in oxygen content in the EDS microanalysis data (see **Fig. 2**). It is also noteworthy that the embedding of ceramic particles facilitates the penetration of C_{60} molecule agglomerates from the surface into the matrix alloy particles.

All of this contributes to the reduction in the particle size of the AlMg6 matrix alloy after the second stage of processing. **Fig. 2** also presents the integral and differential curves characterizing the granulometric composition of the synthesized powder mixtures. The analysis of the results shows that an increase in the ceramic particle content from 10 to 50 wt.% leads to a reduction in d_{50} in the powder mixture from 17.8 to 12.7 μm. On the one hand, this is undoubtedly related to the influence of the increasing proportion of smaller Al_2O_3 particles, whose d_{50} is 18.5 μm. On the other hand, the presence of Al_2O_3 on the surface of the AlMg6 matrix alloy particles inhibits the welding processes between them and intensifies the dispersion processes during ball milling.

It should also be noted that during processing, fragmentation of Al_2O_3 particles occurs. As a result, a significant portion of the Al_2O_3 particles is reduced to micron and submicron sizes (see **Fig. 3, *a***). Another characteristic is the "encapsulation" of ceramic particles by the matrix aluminum alloy. For instance, **Fig. 3, *b*** shows SEM images at various magnifications of an Al_2O_3 particle that was coated with aluminum during processing. Based on the SEM image, visual identification of the particle as a ceramic one is challenging, as it exhibits morphology typical of the matrix alloy particles. However, its end surface displays fracture patterns characteristic of Al_2O_3 ceramics. This feature indicates good adhesion between Al and Al_2O_3, which is expected to positively affect the properties of coatings produced from these powders.

Thus, the obtained multi-reinforced powders are a complex mechanical mixture consisting of agglomerates and micro-sized ceramic particles. Agglomerates are particles of nanocomposite material AlMg6/C_{60} with micro-sized ceramic particles embedded in them, as well

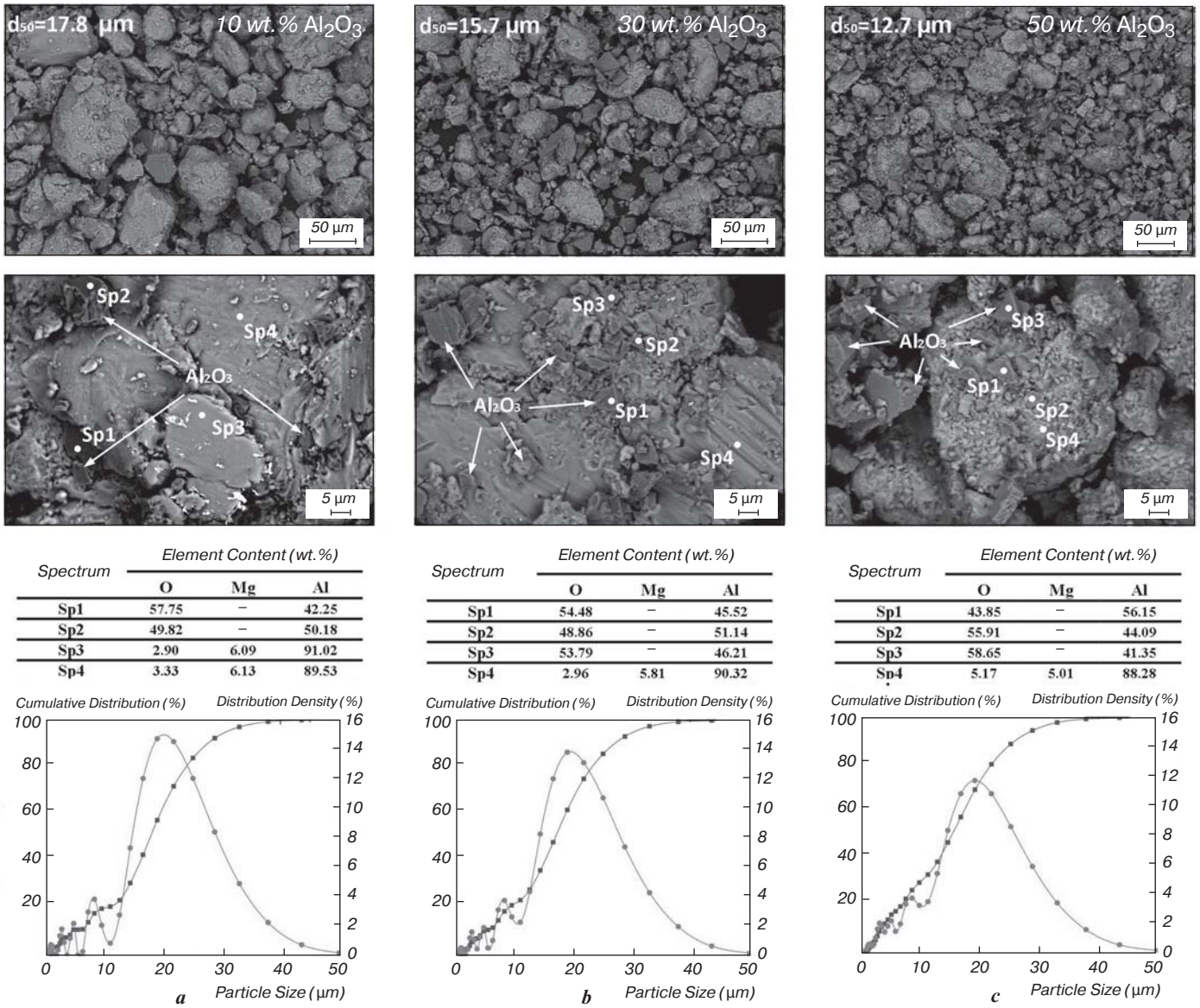

Fig. 2. SEM images, EDS and particle size distribution of multi-reinforced powder mixtures with 10 (*a*), 30 (*b*) or 50 (*c*) wt.% Al_2O_3

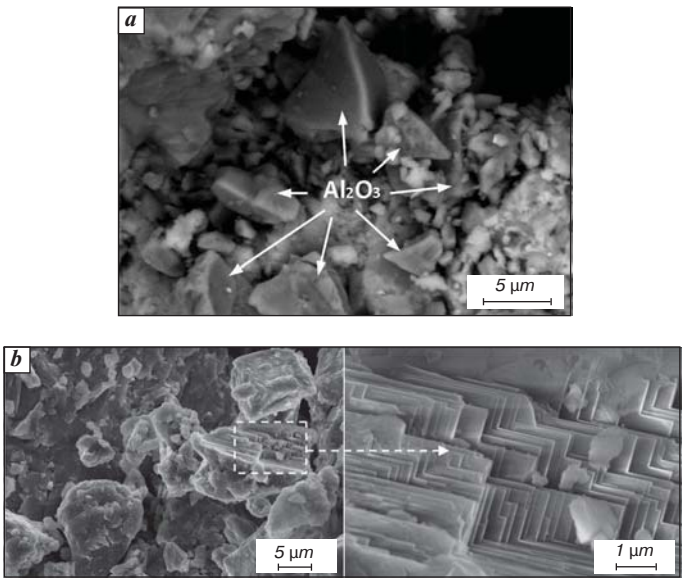

Fig. 3. SEM images illustrating the processes of crushing (*a*) and "enveloping" (*b*) of Al_2O_3 particles

as located on the surface. The concentration of ceramic particles on the surface of agglomerates and embedded in their volume increased with increasing mass fraction of ceramic particles in the initial mixture.

Fig. 4, *a* shows the results of *X*-ray phase analysis of mechanically synthesized powders obtained at the first and second stages of processing.

Analysis of the phase composition of the powders obtained at the first stage of processing shows the presence of peaks corresponding to aluminum. Peaks of C_{60} reinforcing phase were not recorded. On the one hand, this is due to the low content of C_{60} in the powder mixture. On the other hand, it is explained by the microabsorption of *X*-rays in *X*-ray phase analysis of composites reinforced with well dispersed carbon nanostructures [21]. In general, this is typical for aluminum alloys reinforced with carbon structures and at higher concentrations of reinforcing additives [22]. For the multi-reinforced powders obtained in the second stage, the diffraction patterns have a qualitatively similar character. The presence of peaks corresponding to aluminum and ceramic Al_2O_3 particles was observed. Moreover, the intensity of Al_2O_3 peaks increases with the increase of their amount in the powder mixture. The size of coherent scattering regions calculated for AlMg6/C_{60} composite powder obtained at the first stage of processing was ~60 nm. After the second stage of processing the size of coherent scattering regions of AlMg6 alloy is ~40–60 nm. This fact allows predicting the increase of hardness of the matrix alloy, as well as the possibility of formation of nano- or submicrocrystalline structure in coatings formed from these powders by gas dynamic spraying.

Fig. 4, *b* shows the data on the microhardness of particles of synthesized powders depending on the content of Al_2O_3 in the powder mixture. Also, **Fig. 4, *b*** shows the dashed line characterizing the microhardness of the powder of matrix alloy AlMg6 without the addition of reinforcing particles, obtained by the same technological route. Analysis of microhardness change data shows that addition of 0.3 wt.% C_{60} increases the microhardness of powder particles by ~20%. Subsequent reinforcement of powder mixture AlMg6 + 0.3 wt.% C_{60} from 10 to 50 wt.% Al_2O_3 leads to an additional increase in microhardness by ~16-20%. In general, the obtained results confirm the effectiveness of using multi-reinforcing to increase the microhardness of powder particles. This will contribute to the improvement of mechanical properties of the coatings obtained from them.

Fig. 5, *a* shows *X*-ray diffractometry data of coatings formed from multi-reinforced powders by cold gas dynamic spraying. It should be noted that the formation of a coating with a thickness of more than ~10 μm from the powder mixture obtained at the first stage of ball milling (without ceramic particles) was not achieved. This is due to both the limitation of thermal-rate conditions of spraying, provided by the used equipment, and the coarseness of the powder. Therefore, the *X*-ray phase analysis data in **Fig. 5, *a*** are shown only for powder mixtures with 10, 30 or 50 wt.% Al_2O_3.

The diffraction patterns obtained for powders and coatings are somewhat different. For example, for coatings one can observe a decrease in the signal of the peak (111) of the aluminum crystal plane (see **Fig. 5, *a***) compared to

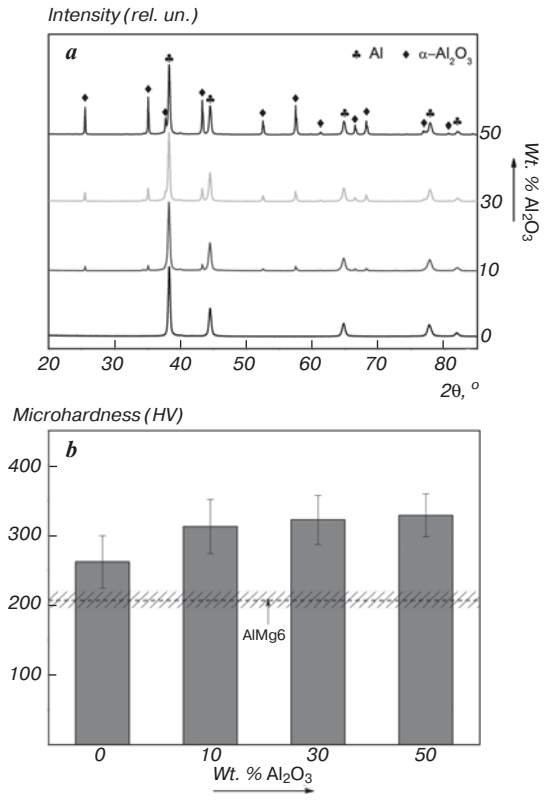

Fig. 4. Results of *X*-ray phase analysis (*a*) and particle microhardness data (*b*) of multi-reinforced powder mixtures with different Al_2O_3 content

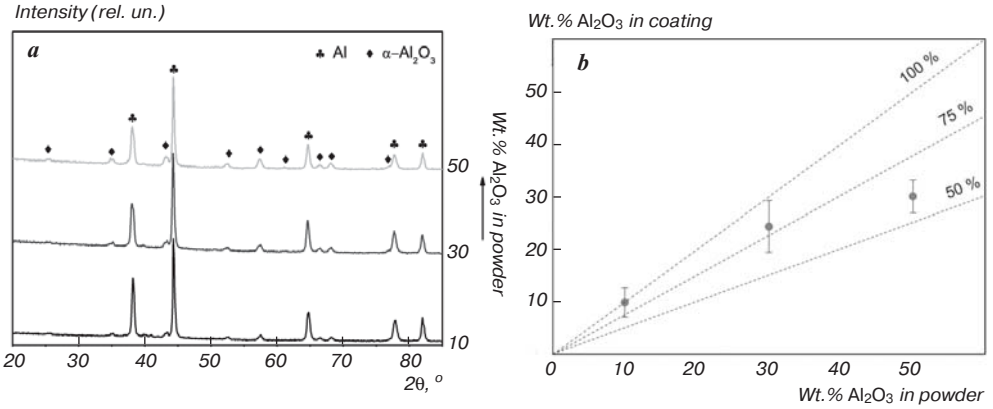

Fig. 5. Results of *X*-ray phase analysis (*a*) and data on Al_2O_3 content (*b*) in coatings

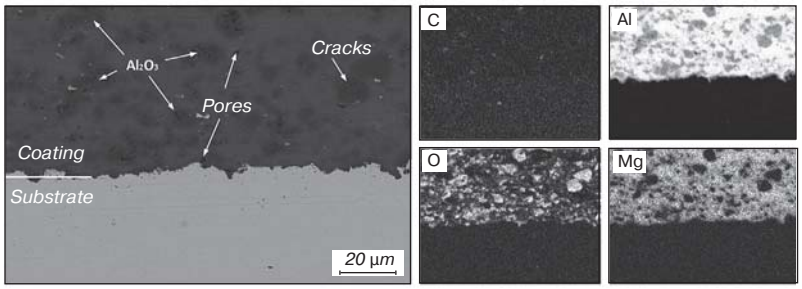

Fig. 6. SEM image of microstructure and EDS mapping data of the coating containing 30 wt.% Al_2O_3

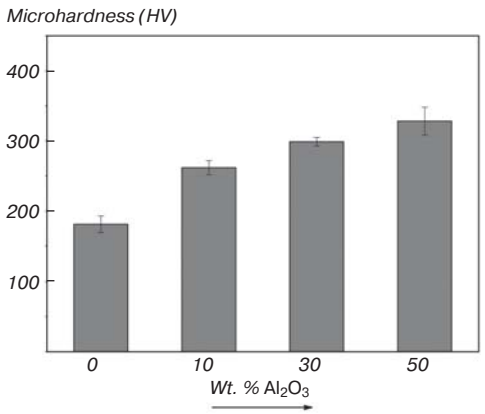

Fig. 7. Microhardness of multi-reinforced coatings with different Al_2O_3 content

powders **(Fig. 4, *a*)**, indicating a reduced amount of crystal planes (111). This suggests a change in the preferential orientation of the matrix alloy grains to a more chaotic orientation during deformation during cold gas dynamic spraying. In addition, the intensity of the peaks corresponding to the ceramic phase of the coating is slightly lower than in the powders. This indicates the incomplete transfer of ceramic particles from the powder mixture into the coating during spraying. Quantitative analysis was performed to evaluate the Al_2O_3 content in the formed coatings. **Fig. 5,** shows the data on the Al_2O_3 content in the coating as a function of the Al_2O_3 content in the powder. For example, when using a powder mixture with 10 wt.% Al_2O_3, the content of the latter amounted to 9.9 ± .8 wt.%. Increasing the content of Al_2O_3 in the powder mixture from 30 to 50 wt.% increased its amount in the coating from 24.2 ± 4.8 wt.% to 30.1 ± 3.1 wt.%. Thus, judging from the quantitative analysis data, under the used conditions of cold gas dynamic spraying, the proportion of ceramic particles transferred to the coating decreased with increasing their content in the powder mixture and amounted to ~99%, ~80% and ~60% for 10, 30 or 50 wt.% Al_2O_3 in the powder, respectively. The crystallite size of the matrix alloy is ~80-120 nm, i.e., the coarsening of the nanocrystalline structure achieved by high-energy ball milling occurs during the spraying process, judging from the *X*-ray diffractometry data.

Fig. 6 shows a typical SEM image of the coating structure as well as EDS mapping data.

The coatings have a fairly homogeneous microstructure, representing densely packed deformed matrix alloy particles with uniformly distributed in their volume carbon nanostructures and ceramic particles of micron and submicron sizes. Occasionally, pores with the size not exceeding 5 microns were fixed in the coating body. In addition, it can be noted that in the process of gas dynamic spraying there is a slight change in the microgeometry of the substrate, which is caused by the erosive effect of the sprayed powder mixture on it. It should also be noted the presence of cracks in the body of micrometer ceramic particles. Apparently, the formation of cracks is caused by the impact of collisions during the coating spraying.

Fig. 7 shows the results of microhardness measurement of coatings with different Al_2O_3 content in the powder mixture.

Thus, the microhardness of the coating monolayer obtained by spraying of AlMg6/C_{60} powder amounted to 181 ± 12 HV. At the same time, the addition of 10 to 50 wt.% Al_2O_3 into the powder composition contributed to the increase in the microhardness of coatings from 261 ± 10 to 328 ± 16 HV.

Conclusions

Nanocrystalline powders based on AlMg6 aluminum alloy, multi-reinforced with nano- and microparticles, were synthesized by two-stage high-energy processing in a planetary ball mill. The synthesized powders were a mechanical mixture with an agglomerated structure. The concentration of Al_2O_3 particles on the surface and inside

the agglomerates increased with increasing mass fraction of ceramic particles in the mixture. Using gas-dynamic spraying, the coatings from the obtained powders were formed, which had a homogeneous microstructure with uniformly distributed strengthening particles in their volume. The amount of ceramic particles transferred into the coating decreased with increasing their content in the powder mixture. A ~2-fold increase in the grain size of the matrix material was observed in the obtained coatings compared to the powders. It was demonstrated that the addition of 10–50 wt.% Al_2O_3 into the powder mixture along with mechanical processing for only 15 minutes increases the microhardness of the coating by ~30–45% as compared to the mono-reinforced material.

Acknowledgments

The research was carried out within the state assignment in the field of scientific activity of the Ministry of Science and Higher Education of the Russian Federation (theme FZUN-2024-0004, state assignment of the VISU).

References

1. Yin S., Cavaliere P., Aldwell B., Jenkins R., Liao H., Li W., Lupoi R. Cold Spray Additive Manufacturing and Repair: Fundamentals and Applications. *Additive Manufacturing*. 2018. Vol. 21. pp. 628–650.

2. Spencer K., Fabijanic D. M., Zhang M.-X. The Use of Al–Al_2O_3 Cold Spray Coatings to Improve the Surface Properties of Magnesium Alloys. *Surface and Coatings Technology*. 2009. Vol. 204, Iss. 3. pp. 336–344.

3. Shockley J. M., Strauss H. W., Chromik R. R., Brodusch N., Gauvin R., Irissou E., Legoux J.-G. In Situ Tribometry of Cold-Sprayed Al-Al_2O_3 composite Coatings. *Surface and Coatings Technology*. 2013. Vol. 215. pp. 350–356.

4. Raoelison R. N., Xie Y., Sapanathan T., Planche M. P., Kromer R., Costil S., Langlade C. Cold Gas Dynamic Spray Technology: A Comprehensive Review of Processing Conditions for Various Technological Developments Till to Date. *Additive Manufacturing*. 2018. Vol. 19. pp. 134–159.

5. Adaan-Nyiak M. A., Tiamiyu A. A. Recent Advances on Bonding Mechanism in Cold Spray Process: A Review of Single-Particle Impact Methods. *Journal of Materials Research*. 2023. Vol. 38. pp. 69–95.

6. Xie X., Yin S., Raoelison R.-nirina, Chen C., Verdy C., Li W., Ji G., Ren Z., Liao H. Al Matrix Composites Fabricated by Solid-State Cold Spray Deposition: a Critical Review. *Journal of Materials Science & Technology*. 2021. Vol. 86. pp. 20–55.

7. Li W., Assadi H., Gaertner F., Yin S. A Review of Advanced Composite and Nanostructured Coatings by Solid-State Cold Spraying Process. *Critical Reviews in Solid State and Materials Sciences*. 2018. Vol. 44, Iss. 2. pp. 109–156.

8. Prusov E. S., Deev V. B., Shurkin P. K., Arakelian S. M. The Effect of Alloying Elements on the Interaction of Boron Carbide with Aluminum Melt. *Non-ferrous Metals*. 2021. No. 1. pp. 7–33.

9. Mansurov Yu. N., Kurbatkina E. I., Buravlev I. Yu., Reva V. P. Features of Structure's Formation and Properties of Composite Aluminum Alloy Ingots. *Non-ferrous Metals*. 2015. No. 2. pp. 40–47.

10. Aborkin A. V., Alymov M. I., Arkhipov V. E., Khrenov D. S. Formation of Heterogeneous Powder Coatings with a Two-Level Micro-and Nanocomposite Structure under Gas-Dynamic Spraying Conditions. *Doklady Physics*. 2018. Vol. 63. pp. 50–54.

11. Evdokimov I. A., Perfilov S. A., Pozdnyakov A. A., Blank V. D., Bagramov R. Kh., Perezhogin I. A., Kulnitsky B. A., Kirichenko A. N., Aksenenkov V. V. Nanostructured Composite Materials Based on Al – Mg Alloy Modified with Fullerene C_{60}. *Inorganic Materials: Applied Research*. 2018. Vol. 9. pp. 472–477.

12. Choi H. J., Shin J. H., Bae D. H. Self-Assembled Network Structures in Al/C_{60} Composites. *Carbon*. 2010. Vol. 48, Iss. 13. pp. 3700–3707.

13. Reshetniak V., Reshetniak O., Aborkin A., Nederkin V., Filippov A. Effect of the Interface on the Compressibility of Substances with Spherical Nano-Inhomogeneities on the Example of Al/C_{60}. *Nanomaterials*. 2022. Vol. 12. 2045.

14. Popova O. I., Glebov V. A., Glebov A. V. Enhancement of Composite Magnets Mechanical Strength by Using of Fullerenes. *Tsvetnye Metally*. 2010. No. 12. pp. 60–63.

15. Fernandez R., Jodoin B. Cold Spray Aluminum–Alumina Cermet Coatings: Effect of Alumina Content. *Journal of Thermal Spray Technology*. 2018. Vol. 27. pp. 603–623.

16. Fernandez R., Jodoin B. Cold Spray Aluminum–Alumina Cermet Coatings: Effect of Alumina Morphology. *Journal of Thermal Spray Technology*. 2019. Vol. 28. pp. 737–755.

17. Kuang Nguyen, Aleshchenko A. S., Guseynov E. R. Understanding the Process of Installing Al + Al_2O_3 Powder Coatings by Cold Gas Dynamic Spraying on Substrates with Different Surface Roughness. *Tsvetnye Metally*. 2021. No. 7. pp. 52–57.

18. Aborkin A., Babin D., Belyaev L., Bokaryov D. Enhancing the Microhardness of Coatings Produced by Cold Gas Dynamic Spraying through Multi-Reinforcement with Aluminum Powders Containing Fullerenes and Aluminum Nitride. *Journal of Manufacturing and Materials Processing*. 2023. Vol. 7, Iss. 6. 203.

19. Aborkin A. V., Arkhipov V. E., Sachkova N. V., Sychev A. E., Alymov M. I. Effect of Al_2O_3 on the Microhardness of AMg2/Graphite Nanocomposite Powder Gas Dynamic Coatings on Aluminum Alloys. *Metal Science and Heat Treatment*. 2019. Vol. 61. pp. 360–365.

20. Aborkin A. V., Alymov M. I., Kireev A. V., Sobol'kov A. V., Arkhipov V. E. Structure and Efficiency of Gas-Dynamic Deposition of Hybrid Coatings Based on a Nanocrystalline Aluminum Matrix. *Metallurgist*. 2018. Vol. 62. pp. 809–814.

21. Popov V. A. X-ray Micro-Absorption Enhancement for non-Agglomerated Nanodiamonds in Mechanically Alloyed Aluminium Matrix Composites. *Physica Status Solidi A*. 2015. Vol. 212. pp. 2722–2726.

22. Aborkin A. V., Alymov M. I., Kireev A. V., Elkin A. I., Sobol'kov A. V. Mechanically Synthesized Composite Powder Based on AMg2 Alloy with Graphite Additives: Particle Size Distribution and Structural-Phase Composition. *Nanotechnologies in Russia*. 2017. Vol. 12. pp. 395–399.

NFM